ARTICLE

Circular Nanopatterns over Large Areas from the Self-Assembly of Block Copolymers Guided by Shallow Trenches

Sung Woo Hong,[†,⊥] Xiaodan Gu,[†,⊥] June Huh,[‡] Shuaigang Xiao,[§] and Thomas P. Russell[†,*]

[†]Department of Polymer Science and Engineering, University of Massachusetts, Amherst, Massachusetts 01003, United States, [‡]Department of Materials Science and Engineering, Yonsei University, 134 Shinchon-dong, Seodaemun-gu, Seoul 120-749, Korea, and [§]Seagate Technology, 47010 Kato Road, Fremont, California 94538, United States. [⊥]These authors equally contributed to this work.

ABSTRACT We report the fabrication of ultradense circular nanolines of block copolymer (BCP) microdomains over macroscopic areas. These lines were generated by the directed self-assembly (DSA) of BCPs on the topographically patterned substrates, where the trenches with circular shape are patterned on a flat substrate. The width of the trench and the distance between trenches are varied for commensurability issues, and difference BCPs are used to demonstrate the generality of this strategy. When a commensurability condition is satisfied, BCPs on the topographically patterned substrates undergo a DSA with solvent annealing, resulting in a flat film with an areal density amplification of the circular patterns over large areas. The methodology described here may provide an easy approach to high densities of circularly shaped nanopatterns for data storage device manufacturing.

KEYWORDS: block copolymer · solvent annealing · trench · areal density · circular patterns

During the past decade, much effort has been devoted to enhance the areal density of bits for data storage applications. Optical and e-beam lithographies have traditionally been used for fabricating patterns with small feature sizes. However, optical lithography has an intrinsic technological diffraction limit as to the smallest feature size achievable.[1,2] E-beam lithography, on the other hand, with exceptional spatial resolution, is a very promising technique to achieve sub-100 nm patterns. However, e-beam lithography is a high-cost, serial writing process with too low through-put for high-volume production.[3] Highly parallel techniques, such as nanoimprint lithography, have been developed that overcome the cost and through-put impediments,[4] but they still require the fabrication of a very costly master that must be produced by an alternative process.[3] Nonetheless, with a master in hand, nanoimprint lithography will be the technique of choice in the future for the large-scale fabrication of nanoarrays or patterns of nanoscopic elements.

The directed self-assembly (DSA) of block copolymers (BCPs), a highly parallel process where the orientation and placement of BCP microdomains can be controlled by topographical or chemical patterning of surfaces,[5−17] offers a simple, robust, and rapid route to generate nanostructured materials. Moreover, features sized down to 3 nm have already been demonstrated with the potential for extending this to even smaller sizes, and as such, the limitation in size scale has been overcome. Trench-patterned substrates have been extensively studied to control the lateral ordering of the nanoscopic BCP microdomains in thin films.[6−8,10−13,15,16] However, there has been little effort on generation of line patterns on circular geometries over large areas, which is of most relevance to industry.[3] In addition, most studies have focused on a geometry where the depth of the trench (d_t) was larger than the center-to-center distance between BCP microdomains in the bulk ($L_{2,B}$),[6−8,10−13,15,16] which limits the grain size to the width of the trench (w_t), as shown in Figure 1A.

Recently, Russell and co-workers demonstrated a DSA of BCPs using the faceted substrates.[18] The self-assembly of BCPs was guided by the small amplitude ridges of the facets rather than by a confinement effect between facets. This DSA produced a single grain of BCP microdomains over macroscopic length scales. Here, by mimicking this faceted substrate, we use shallow trenches in the form of a circle to direct the self-assembly of BCPs. As shown in Figure 1B, the depth of the shallow circular trench (d_{sct}) is designed to be much smaller than $L_{2,B}$. In addition,

* Address correspondence to russell@mail.pse.umass.edu.

Received for review December 9, 2010 and accepted February 25, 2011.

Published online March 11, 2011
10.1021/nn103401w

© 2011 American Chemical Society

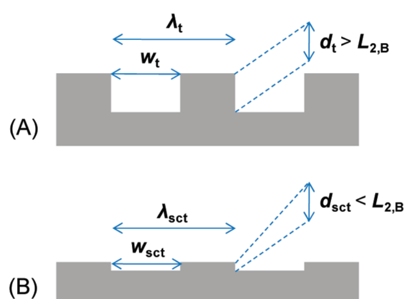

Figure 1. Graphical illustrations of (A) the conventional trenches and (B) the shallow circular trenches prepared in this work, where λ is the width between trenches, w is the width of the trench, d is the depth of the trench, and $L_{2,B}$ is the center-to-center distance between BCP microdomains in the bulk.

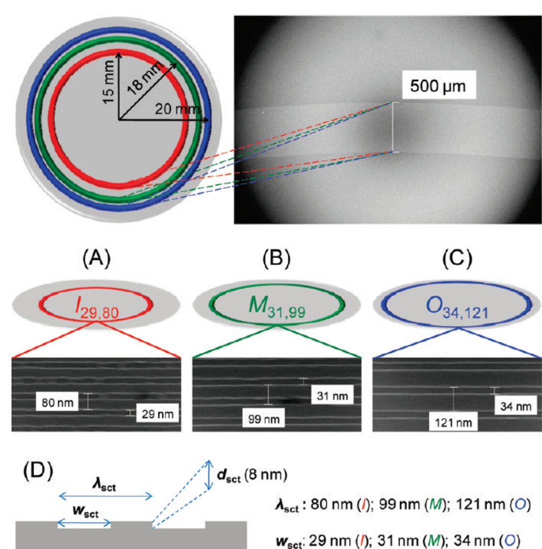

Figure 2. Graphical illustrations and the SEM images of three different kinds of circularly patterned areas, and the magnifications of (A) inner ($I_{29,80}$), (B) middle ($M_{31,99}$), and (C) outer ($O_{34,121}$) rim regions. (D) Graphical illustrations for d_{sct}, λ_{sct}, and w_{sct}.

the width of the shallow circular trench (w_{sct}) and the distance between the shallow circular trenches (λ_{sct}) are varied to address commensurability issues. We describe a simple method to obtain circular nanopatterns of BCPs with a well-defined orientation over macroscopic areas using the shallow circular trenches prepared in this study.

RESULTS AND DISCUSSION

Figure 2 shows schematics and scanning electron microscope (SEM) images of a topographically patterned substrate that contains three different kinds of circularly patterned regions. The inner rim region ($I_{29,80}$), the middle rim region ($M_{31,99}$), and the outer rim region ($O_{34,121}$) have the same width of 500 μm, but each rim region has its own topography: $I_{29,80}$, $M_{31,99}$, and $O_{34,121}$ have widths of 29, 31, and 34 nm with distances between the trenches of 80, 99, and 121 nm, respectively. Thin films of cylinder-forming polystyrene-*b*-poly(ethylene oxide) (PS-*b*-PEO) (M_n = 26.5 kg/mol with a center-to-center domain spacing of the solvent-annealed cylindrical PEO microdomains oriented normal to the surface ($L_{1,+}$) = 32.3 nm) with a film thickness of 38.0 nm (on a smooth flat surface) were prepared on these circularly patterned substrates and then exposed to THF and water to induce lateral ordering of the PS-*b*-PEO.

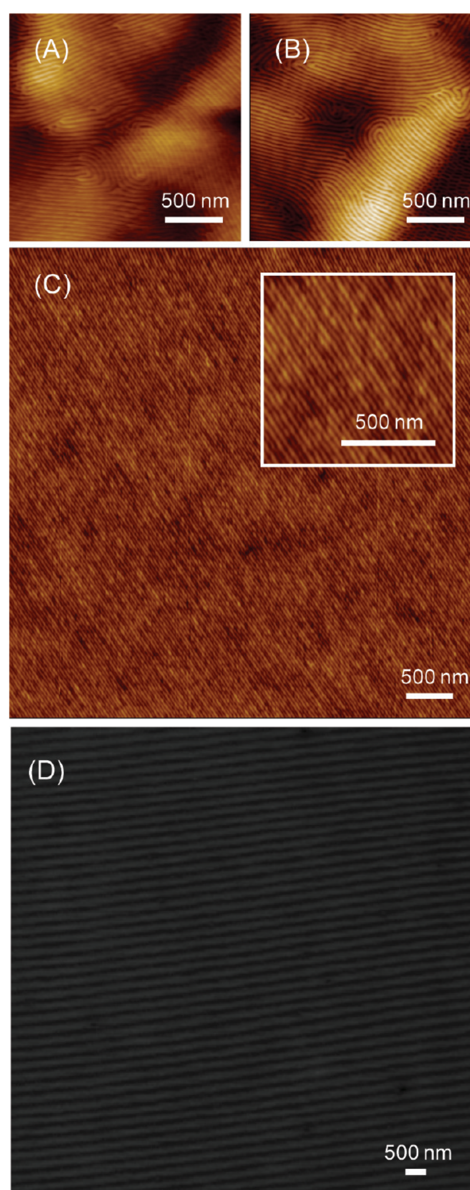

Figure 3. SFM height images of the defect-free faceted substrate. (C) Cross sectional line scan from (B). SFM height images of PS-*b*-PEO (M_n = 26.5 kg/mol) thin films with a thickness of 38.0 nm on (A) $I_{29,80}$, (B) $O_{34,121}$, and (C) $M_{31,99}$ after solvent annealing. The inset in (C) is the magnification of (C). (D) Moiré patterns of a highly ordered PS-*b*-PEO thin film on $M_{31,99}$. All the scale bars are 500 nm.

Figure 3 shows scanning force microscopy (SFM) images of PS-*b*-PEO thin films on $I_{29,80}$, $M_{31,99}$, and

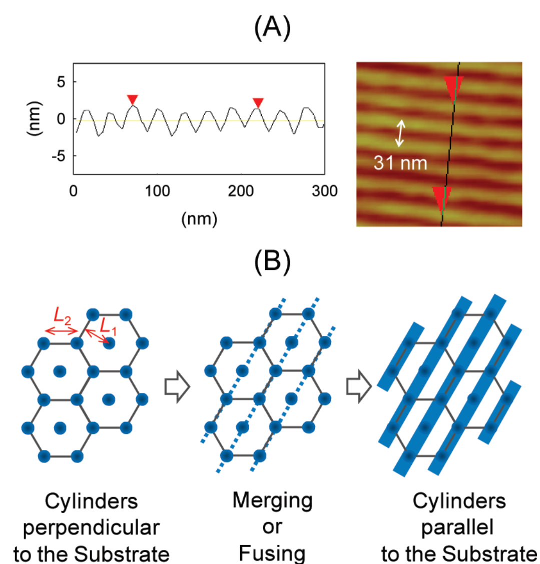

Figure 4. (A) Cross sectional line scan of a highly ordered PS-*b*-PEO thin film on $M_{31,99}$ from Figure 3C. (B) Graphical presentation of the proposed mechanism for the transformation of PEO microdomains from *perpendicular* to *parallel* on $M_{31,99}$ as solvent annealing proceeds.

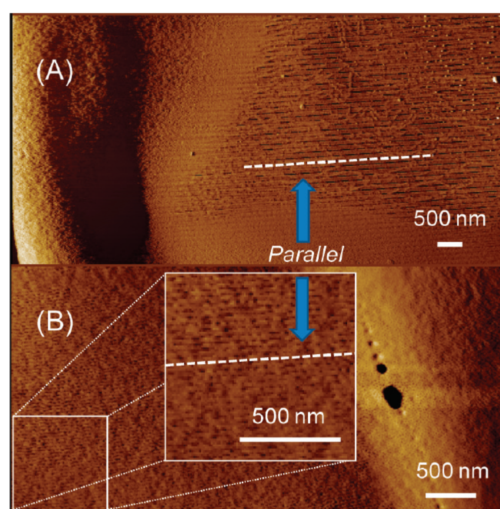

Figure 5. (A) SFM phase image of interfacial region between the remaining PS-*b*-PEO thin film and the underlying substrate. (B) SFM phase image translated to the left from (A) without any rotation of sample stage. The inset in (B) is the magnification of the left side. All the scale bars are 500 nm.

$O_{35,121}$ after solvent annealing. When the solvent annealing was conducted on $I_{29,80}$ (or $O_{35,121}$), cylindrical PEO microdomains oriented parallel to the substrate were randomly aligned, resulting in the classic fingerprint-type patterns, as shown in Figure 3A and B. This is quite similar to that seen for thin films solvent-annealed on a flat Si substrate (see Figure S1 in the Supporting Information for the SFM image of PS-*b*-PEO thin film prepared on a flat Si substrate), indicating that the circular trenches on $I_{29,80}$ (or $O_{35,121}$) did not guide the self-assembly of PS-*b*-PEO effectively. However, the solvent annealing of the PS-*b*-PEO thin film on $M_{31,99}$ resulted in a morphology of highly ordered and aligned PEO microdomains oriented parallel to the surface, as shown in Figure 3C. Moiré patterns were used to directly characterize the orientation, grain size, and dislocations in the arrays of BCP microdomains (see Figure S2 in the Supporting Information for the typical examples for Moiré patterns).[19] Figure 3D shows Moiré patterns of a highly ordered PS-*b*-PEO thin film on $M_{31,99}$ measured by SFM. The line patterns are evident, indicating the formation of a large single grain with few dislocations or misorientations. This result is independent of position over the entire area of $M_{31,99}$, which demonstrates that the DSA of the PS-*b*-PEO on the circular trenches significantly enhanced the long-range lateral ordering. Since the depth of the circular trench (8 nm) was much smaller than the center-to-center distance between BCP microdomains, the surface of the BCP films is flat over large areas.

Recently, we found that, when the cylinder-forming PS-*b*-PEO thin films were solvent-annealed with THF and water, arrays of hexagonally packed PEO microdomains oriented normal to the surface were obtained at the early stage of solvent annealing. With further solvent annealing, these PEO microdomains began to merge with each other, transforming the morphology into PEO microdomains oriented parallel to the surface.[20] Theoretically, the center-to-center distance between PEO microdomains oriented parallel to the surface of $M_{31,99}$ ($L_{2,\|}$) should equal $L_{2,+}$ (the center-to-center distance between the solvent-annealed cylindrical PEO microdomains oriented normal to the surface). However, when the SFM image of line patterns of PS-*b*-PEO on $M_{31,99}$ is cross-sectioned, as shown in Figure 4A, $L_{2,\|}$ is found to be 31 nm, which is close to $L_{1,+}$ (the center-to-center domain spacing of the solvent-annealed cylindrical PEO microdomains oriented normal to the surface), not $L_{2,+}$. This suggests that hexagonally packed PEO microdomains oriented normal to the surface of $M_{31,99}$ merge along the (1 0) planes (see Figure S3 in the Supporting Information for the direction of merging). However, the fused PEO microdomains are in a compressed state, where the elastic penalty arising from incommensurability is compensated by the interaction between trench and polymer, as well as that between solvent vapor and selective block. Figure 4B shows a schematic diagram of the mechanism underpinning the transformation in the orientation of the cylindrical PEO microdomains from *perpendicular* to *parallel* to $M_{31,99}$ as solvent annealing proceeds.

The distance between the circular trenches on $M_{31,99}$ (99 nm) is commensurate with $L_{1,+}$. Here, a section of the PS-*b*-PEO thin film on $M_{31,99}$ was removed by dichloromethane, and the interfacial region between the remaining PS-*b*-PEO thin film and the exposed underlying substrate was investigated. Figure 5A shows the SFM image from this interfacial region,

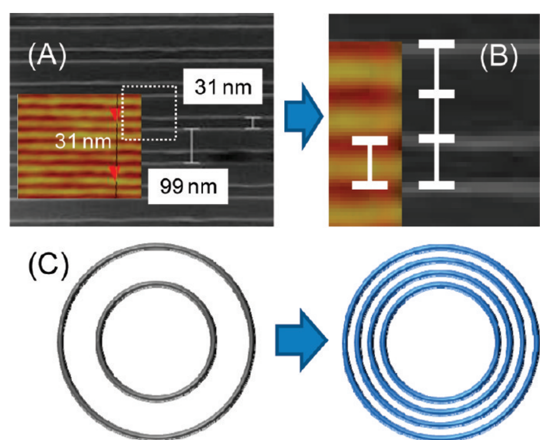

Figure 6. (A) Superposition of the line patterns (SFM image) from PS-*b*-PEO on the line patterns (SEM image) from $M_{31,99}$. (B) Magnification of the white dotted box in (A). (C) Schematic diagram representing the areal density multiplication of circular patterns by a factor of 3.

where the line patterns on the underlying substrate are seen. When the line patterns are cross-sectioned (see Figure S4 in the Supporting Information for the cross-sectional image of Figure 5A), it is seen that the exposed line patterns originate with the $M_{31,99}$ substrate. When the sample stage was translated, the line patterns from the PS-*b*-PEO thin film were observed. They were slightly damaged during the solvent treatment, as shown in Figure 5B. It should be noted that the sample stage was only translated with no rotation so as to directly compare the orientation of the line patterns from Figure 5A and B (see Figure S5 in the Supporting Information for the translation of sample stage). When the line patterns of $M_{31,99}$ in Figure 5A and those of PS-*b*-PEO in Figure 5B are compared, it is seen that they are parallel to each other, as indicated in Figure 5. This demonstrates that the cylindrical PEO microdomains are ordered and oriented along the direction of circular patterns of $M_{31,99}$. Previously, Ruiz *et al*. reported a directed block copolymer assembly method for feature density multiplication using lithographically defined chemically prepatterned surfaces,[21] and Bita *et al*. studied a topographical graphoexpitaxy technique for BCPs using two-dimensional periodic templates patterned with nanoposts.[22] In this study, it is also found that $L_{2J\|}$ on $M_{31,99}$ is three times smaller than the distance between trenches on $M_{31,99}$, effectively tripling the areal density of the circular trench, as shown in Figure 6. All of these results indicate that the circular trenches on $M_{31,99}$ can guide the self-assembly of PS-*b*-PEO along the direction of circular patterns of $M_{31,99}$ over macroscopic areas. However, in the case of $I_{29,80}$ or $O_{34,121}$, since the distance between circular trenches is not commensurate with $L_{1,+}$, the trench patterns on $I_{29,80}$ (or $O_{34,121}$) could not effectively guide the self-assembly of PS-*b*-PEO, resulting in the fingerprint patterns, as shown in Figure 3A and B. Table 1 summarizes the results of the self-assembly of PS-*b*-PEO on $I_{29,80}$, $M_{31,99}$, and $O_{34,121}$.

TABLE 1. Summary of the Results of the Self-Assembly of PS-*b*-PEO on $I_{29,80}$, $M_{31,99}$, and $O_{34,121}$

	$\lambda_{sch}{}^{a}/w_{sch}{}^{b}$	$w_{sch}/L_{1,B}{}^{c}$	$\lambda_{sch}/L_{1,B}$	long-range lateral ordering
$I_{29,80}$	2.79 (≈integer)	0.89 (≈integer)	2.49 (≠integer)	failed
$M_{31,99}$	3.19 (≈integer)	0.95 (integer)	3.04 (integer)	successful
$O_{34,121}$	3.90 (≈integer)	1.04 (integer)	3.72 (≠integer)	failed

[a] Distance between shallow circular trenches. [b] Width of shallow circular trench. [c] Center-to-center domain spacing of cylindrical PEO microdomains in bulk.

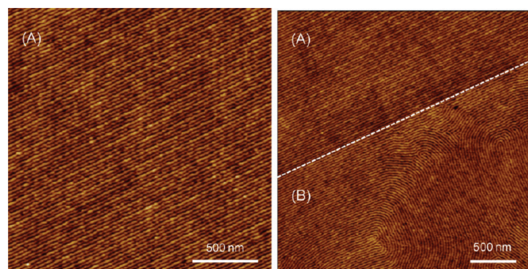

Figure 7. SFM height images of a PS-*b*-P2VP (M_n = 34.0 kg/mol) thin film with a thickness of 36.5 nm on (A) $I_{29,80}$ and (B) nonpatterned surface after solvent annealing. All the scale bars are 500 nm.

Finally, we used different BCPs to demonstrate the generality of this strategy. Thin films of cylinder-forming PS-*b*-P2VP (M_n = 34.0 kg/mol; with a center-to-center domain spacing of the solvent-annealed cylindrical P2VP microdomains oriented normal to the surface = 27.2 nm) with a thickness of 36.5 nm (on a smooth flat surface) were prepared on the circularly patterned substrates and then solvent-annealed with THF and water. Highly ordered and oriented PS-*b*-P2VP microdomains were obtained on $I_{29,80}$ with the amplification of the areal density of the circular trench by a factor of 3, while fingerprint patterns were found on the non-patterned surface, as shown in Figure 7. This underscores the generality of the strategy for different BCPs and indicates that commensurability is the only condition that needs to be satisfied to amplify the areal density of the pattern. By translating the sample, multiple measurements were taken from three different areas, as shown in Figure 8, which shows that the lateral ordering is independent of position over the entire area of $I_{29,80}$, and the direction of the line patterns of $I_{29,80}$ is parallel to that of PS-*b*-P2VP. It should also be noted that, since the depth of the shallow circular trench (8 nm) was designed to be much smaller than the center-to-center distance between BCP microdomains in the bulk, the surface of the BCPs are flat over large areas. In general, cylindrical microdomains oriented parallel to the surface could not be as ideal as lamellar microdomains oriented perpendicular to the surface for data storage device fabrications due to lower etching contrast issues arising from their limited aspect ratio. However, etching

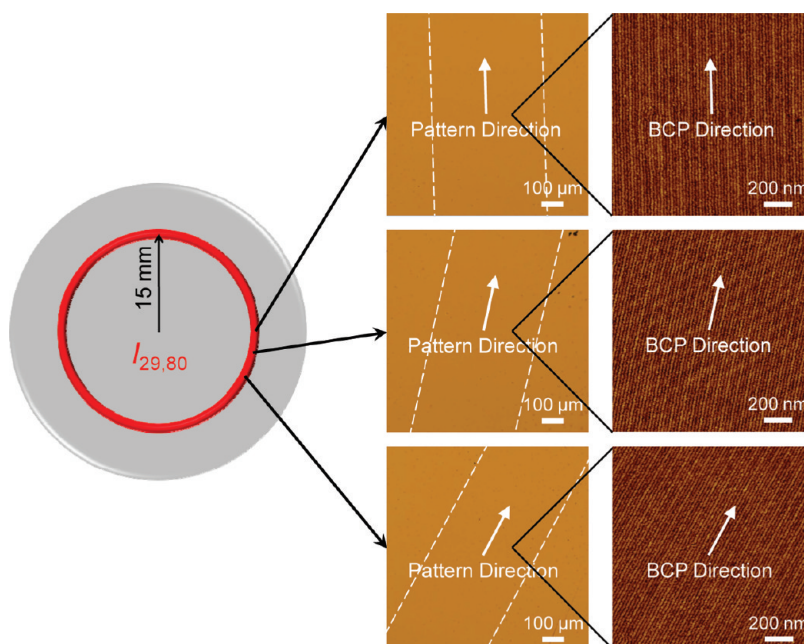

Figure 8. OM images and SFM height images of a PS-*b*-P2VP (M_n = 34.0 kg/mol) thin film with a thickness of 36.5 nm on $l_{29,80}$. Three different areas are randomly selected from the annealed BCP thin film.

resistance of cylindrical microdomains can be significantly improved if BCP thin films are reconstructed and backfilled with Si-containing materials, and backfilled parts are converted into inorganic materials upon UV exposure.[23] In addition, it has been reported that BCPs contacting pyridine groups or ether groups can be complexed with metal ions, and the complexed block can be converted into inorganic materials upon UV exposure,[24] which can also overcome poor etching characteristics of cylindrical microdomains.

CONCLUSIONS

In summary, we have demonstrated the DSA of BCPs to produce ultradense circular arrays of nanoscopic elements. BCPs on the topographically patterned substrates undergo a DSA with solvent annealing, resulting in a flat BCP film with an areal density multiplication of the circular patterns over large areas. We have shown an amplification of pattern by a factor of 3, but, on the basis of the results of commensurability studies, a much larger amplification could be also achieved. The methodology described here may provide an easy approach to high densities of circularly shaped nanopatterns that can, in turn, be used to generate a topographic pattern to orient BCP microdomains normal to the surface, as seen with faceted surfaces, which is of interest for data storage device manufacturing.

EXPERIMENTAL SECTION

Topographically Patterned Substrates. Si (100) wafers capped with a 2 nm native oxide layer were cleaned with oxygen ash. A 50 nm thick film of EB resist (ZEP520A) was spin-coated onto a Si substrate and baked at 180 °C for 3 min. The ZEP520A was then patterned using a rotary-stage electron beam system at 50 keV, creating the circumferential line patterns with various pitches. After development, an oxygen plasma process (30 W, 2 mTorr, 30 sccm) is used to clean the resist residue at the bottom of the trenches. Then a CF_4 reactive-ion etch (80 W, 20 mTorr, 30 sccm CF_4, 30 sccm Ar) was used to transfer the line pattern into the underlying Si substrate at depths of 8 nm.

Solvent Annealing. Thin films of BCPs were prepared by spin-coating the solutions of PS-*b*-PEO (M_n = 26.5 kg/mol; purchased from Polymer Source) and benzene or the solutions of PS-*b*-P2VP (M_n = 34.0 kg/mol; purchased from Polymer Source) and toluene onto the topographically patterned substrates, where the film thickness was controlled by adjusting the concentration of solution and the speed of spin-coating. Solvent annealing was performed in THF and water vapor environment: a preswelling of the BCP polymer film in water vapor was performed to prevent dewetting during the solvent annealing, followed by a solvent annealing in THF and water vapor to prepare well-developed nanostructures.

Characterization. The surface topographies of PS-*b*-PEO thin films on the topographically patterned substrate were imaged by scanning force microscopy (Digital Instruments, Nanoscope III) in the tapping mode.

Acknowledgment. This work was supported by the U.S. Department of Energy (DOE), Office of Basic Energy Sciences, the NSF-supported Materials Research Science and Engineering Center, and the NSF-supported Center for Hierarchical Manufacturing and Seagate Technologies. This work was also supported by the Korea Science and Engineering Foundation (KOSEF) grant funded by the Korea government (MEST).

Supporting Information Available: This material is available free of charge *via* the Internet at http://pubs.acs.org.

REFERENCES AND NOTES

1. Semiconductor Industry Association. *International Technology Roadmap for Semiconductor*, 2005 ed.; Semiconductor Industry Association: San Hose, CA, 2005.
2. Bang, J.; Jeong, U.; Rue, D.; Russell, Y.; Hawker, T. P.; Block, C. J. Copolymer Nanolithography: Translation of Molecular Level Control to Nanoscale Patterns. *Adv. Mater.* **2009,** *21*, 1–24.
3. Sbiaa, R.; Piramanayagam, S. N. Patterned Media Towards Nano-Bit Magnetic Recording: Fabrication and Challenges. *Recent Pat. Nanotechnol.* **2007,** *1*, 29–40.
4. Chou, S. Y. Nanoimprint Lithography. US 5772905, 1998.
5. Rockford, L.; Liu, Y.; Mansky, P.; Russell, T. P.; Yoon, M.; Mochrie, S. G. J. Polymers on Nanoperiodic, Heterogeneous Surfaces. *Phys. Rev. Lett.* **1999,** *82*, 2602–2605.
6. Segalman, R. A.; Yokoyama, H.; Kramer, E. J. Graphoepitaxy of Spherical Domain Block Copolymer Films. *Adv. Mater.* **2001,** *13*, 1152–1155.
7. Kim, S. O.; Solak, H. H.; Stoykovich, M. P.; Ferrier, N. J.; De Pablo, J. J.; Nealey, P. F. Epitaxial Self-Assembly of Block Copolymers on Lithographically Defined Nanopatterned Substrates. *Nature* **2003,** *424*, 411–414.
8. Sundrani, D.; Darling, S. B.; Sibener, S. J. Guiding Polymers to Perfection Macroscopic Alignment of Nanoscale Domains. *Nano Lett.* **2004,** *4*, 273–276.
9. Edwards, E. W.; Montague, M. F.; Solak, H. H.; Hawker, C. J.; Nealey, P. F. Precise Control Over Molecular Dimensions of Block-Copolymer Domains Using the Interfacial Energy of Chemically Nanopatterned Substrates. *Adv. Mater.* **2004,** *16*, 1315–1319.
10. Black, C. T. Self-Aligned Self Assembly of Multi-Nanowire Silicon Field Effect Transistors. *Appl. Phys. Lett.* **2005,** *87*, 163116-1-3.
11. Stoykovich, M. P.; Nealey, P. F. Block Copolymers and Conventional Lithography. *Mater. Today* **2006,** *9*, 20–29.
12. Cheng, J. Y.; Ross, C. A.; Smith, H. I.; Thomas, E. L. Templated Self-Assembly of Block Copolymers: Top-Down Helps Bottom-Up. *Adv. Mater.* **2006,** *18*, 2505–2521.
13. Jung, Y. S.; Ross, C. A. Orientation-Controlled Self-Assembled Nanolithography Using AaPolystyrene-Polydimethylsiloxane Block Copolymer. *Nano Lett.* **2007,** *7*, 2046–2050.
14. Chai, J.; Buriak, J. M. Using Cylindrical Domains of Block Copolymers to Self-Assemble and Align Metallic Nanowires. *ACS Nano* **2008,** *2*, 489–501.
15. Park, S.-M.; Rettner, C. T.; Pitera, J. W.; Kim, H.-C. Directed Self-Assembly of Lamellar Microdomains of Block Copolymers Using Topographic Guiding Patterns. *Macromolecules* **2009,** *42*, 5895–5899.
16. Jeong, S.-J.; Kim, J. E.; Moon, H.-S.; Kim, B. H.; Kim, S. M.; Kim, J. B.; Kim, S. O. One-Dimensional Metal Nanowire Assembly *via* Block Copolymer Soft Graphoepitaxy. *Nano Lett.* **2009,** *9*, 2300–2305.
17. Xu, J.; Park, S.; Wang, S.; Russell, T. R.; Ocko, B. M.; Cheeco, A. Directed Self-Assembly of Block Copolymers on Two-Dimensional Chemical Patterns Fabricated by Electro-Oxidation Nanolithography. *Adv. Mater.* **2010,** *22*, 2268–2272.
18. Park, S.; Lee, D. H.; Xu, J.; Kim, B.; Hong, S. W.; Jeong, U.; Xu, T.; Russell, T. P. Macroscopic 10 Terabit/In^2 Arrays from Block Copolymers with Lateral Order. *Science* **2009,** *323*, 1030–1033.
19. Hexemer, A.; Stein, G. E.; Kramer, E. J.; Magonov, S. Block Copolymer Monolayer Structure Measured with Scanning Force Microscopy Moiré Patterns. *Macromolecules* **2005,** *38*, 7083–7089.
20. Unpublished results.
21. Ruiz, R.; Kang, H.; Detcheverry, F. A.; Dobisz, E.; Kercher, D. S.; Albrecht, T. R.; De Pablo, J. J.; Nealey, P. F. Density Multiplication and Improved Lithography by Directed Block Copolymer Assembly. *Science* **2008,** *321*, 936–939.
22. Bita, I.; Yang, J. K. W.; Jung, Y. S.; Ross, C. A.; Thomas, E. L.; Berggren, K. K. Graphoepitaxy of Self-Assembled Block Copolymer on Two-Dimensional Periodic Patterned Templates. *Science* **2008,** *321*, 939–943.
23. Park, S.; Kim, B.; Wang, J.-Y.; Russell, T. P. Fabrication of Highly Ordered Silicon Oxide Dots and Stripes from Block Copolymer Thin Films. *Adv. Mater.* **2008,** *20*, 681–685.
24. Mistark, P. A.; Park, S.; Yalcin, S. E.; Lee, D. H.; Yavuzcetin, O.; Tuominen, M. T.; Russell, T. P.; Achermann, M. Block-Copolymer-Based Plasmonic Nanostructures. *ACS Nano* **2009,** *3*, 3987–3992.